LA-UR- 09-01139

Approved for public release;
distribution is unlimited.

Title:	Suppression of Auger Recombination in "Giant" Core/Shell Nanocrystals
Author(s):	Florencio Garcia Santamaria Yongfen Chen Javier Vela Richard D. Schaller Jennifer A. Hollingsworth Victor I. Klimov
Intended for:	Submission for publication in an international journal

Los Alamos
NATIONAL LABORATORY
EST.1943

Form 836 (7/06)

Suppression of Auger Recombination in "Giant" Core/Shell Nanocrystals

Florencio García-Santamaría, Yongfen Chen, Javier Vela, Richard D. Schaller, Jennifer A. Hollingsworth, and Victor I. Klimov*

Chemistry Division and Center for Integrated Nanotechnologies, Los Alamos National Laboratory, Los Alamos, NM 87545, USA.

* To whom correspondence should be addressed. E-mail address: klimov@lanl.gov

One-Sentence Summary: "Giant" semiconductor nanocrystals show evidence for very significant, possibly complete, suppression of Auger recombination, which allows for efficient optical gain with a very large bandwidth (>500 meV) and unprecedented low excitation thresholds (<30 $\mu J\ cm^{-2}$).

Abstract: Many potential applications of semiconductor nanocrystals are hindered by non-radiative Auger recombination wherein the electron-hole (exciton) recombination energy is transferred to a third charge carrier. This process severely limits the lifetime and bandwidth of optical gain, leads to large nonradiative losses in light emitting diodes and photovoltaic cells, and is believed to be responsible for intermittency ("blinking") of emission from single nanocrystals. The development of nanostructures in which Auger recombination is suppressed has been a longstanding goal in colloidal nanocrystal research. Here, we demonstrate that such suppression is possible using so-called "giant" nanocrystals that consist of a small CdSe core and a thick CdS shell. These nanostructures exhibit a very long biexciton lifetime (~10 ns) that is likely dominated by radiative decay instead of non-radiative Auger recombination. As a result of suppressed Auger recombination, even high-order multiexcitons exhibit high emission efficiencies, which allows us to demonstrate optical amplification with an extraordinarily large bandwidth (>500 meV) and record low excitation thresholds.

Colloidal semiconductor nanocrystals (NCs) have been the subject of intense research due to potential applications in low-threshold lasers, biological tags, third-generation photovoltaics, and light emitting diodes (LEDs) (*1, 2*). All of these technologies can benefit from the unique properties of NCs such as a size-tunable energy gap, high photoluminescence (PL) quantum yields, good stability, and chemical processibility. Many of these potential applications are, however, hindered by Auger recombination, wherein the energy of one electron-hole pair (exciton) is nonradiatively transferred to another charge carrier (*3*). In NCs, this process occurs on sub-nanosecond (sub-ns) timescales, and reduces optical gain lifetimes (*4*), restricts the available time to extract multiple excitons generated via carrier multiplication (*5*), limits LED brightness due to the buildup of charged NCs (*6*) and leads to PL intermittency ("blinking") that is typically observed in single-NC studies (*7, 8*).

While the physics underlying Auger recombination in NCs is still not fully understood, general considerations suggest that the rate of this process is directly dependent upon the strength of carrier-carrier Coulomb coupling and the degree of spatial overlap between the electron and hole wave functions involved in the Auger transition (*9-11*). Previous approaches to reducing Auger recombination rates have utilized the manipulation of both of these parameters. For example, using elongated NCs (quantum rods), one can separate interacting excitons along the rod axis, which leads to decreased exciton-exciton Coulomb coupling (*12*). Also, one can reduce the rate of Auger transitions by separating electrons and holes between the core and the shell regions of type-II or inverted core-shell heterostructured NCs (*13, 14*).

Although these previous approaches did show a moderate reduction of the Auger recombination rate (typically by a factor of no more than 2), this mechanism still dominated multiexciton dynamics. Therefore, a longstanding goal in NC research yet to be achieved is the

development of nanostructures with a complete suppression of Auger recombination. Here, we demonstrate for the first time that a new class of NCs consisting of a CdSe core and a thick CdS shell show very significant, likely complete, suppression of Auger recombination. Further, long multiexciton lifetimes, combined with large absorption cross-sections of these nanostructures, allow us to demonstrate the lowest reported threshold for amplified spontaneous emission (ASE) in NCs, as well as a broad-band optical gain (extending from 2.0 to 2.6 eV) that arises from multiexcitons of up to at least order 9.

In our initial synthetic work on so-called "giant" NCs (g-NCs), we attempted to improve chemical- and photo-stability by isolating a small emitting core from its chemical environment with a thick shell (single-composition or graded composition) of a wider-gap material and to effectively create a solution-phase structural mimic of an epitaxial quantum dot (*15*). It was hypothesized that this approach would lead to suppressed PL blinking, as the thick shell would prevent carriers from leaving the NC, inhibiting the formation of non-emitting charged NCs (*7, 8*). The synthesized g-NCs indeed exhibited greatly improved chemical- and photo-stability and suppressed blinking (*15*), a result that has been confirmed by an independent study of similar structures (*16*).

Here, we address the fundamental issue of non-radiative Auger recombination by revealing for the first time the unprecedented dynamic and spectral properties of multiexcitons in g-NCs. Specifically, we investigate g-NCs with a 1.5-nm CdSe core radius and a thick shell, comprising up to 19 CdS monolayers (Figs. 1A,B); see also Fig. S1 in the Supplementary Online Materials (SOM). We obtain PL quantum yields for these samples of ~50 to 60%. The emission energy of the CdSe seed particles is ~2.2 eV (Fig. 1C), shifting to the red by more than 200 meV upon deposition of the thick CdS shell (Fig. 1D). Based on the energy offsets at the CdSe/CdS

interface (Fig. 1E), this shift occurs mostly as a consequence of electron delocalization into the shell region, while the hole remains primarily confined to the core (Fig. 1F). The PL red shift is accompanied by a significant increase (almost 100-fold) of the absorption cross-section at high spectral energies (>2.4 eV) because in g-NCs high-frequency absorption is dominated by the CdS shell, which accounts for ~99% of the nanostructure volume.

To study exciton population dynamics, we time-resolve the PL using time-correlated single-photon counting (time resolution is 50 ps). The samples are excited by 200 fs pulses at 3.1 eV. An average initial NC occupancy following photoexcitation, $\langle N_0 \rangle = \langle N(t = 0) \rangle$, can be estimated from $\langle N_0 \rangle = \sigma j_p$, where σ is the NC absorption cross-section and j_p is the per-pulse photon fluence. We start our measurements with a sample of standard CdSe NCs overcoated with a thin ZnS shell (*17*) (referred to here as "reference") that emit at approximately the same wavelength as the g-NCs under investigation.

The pump-intensity dependent PL dynamics of the reference sample show trends that are typically observed for NCs (Fig. 2A). At low pump fluences ($\langle N_0 \rangle << 1$), we observe a relatively slow, ~30-ns decay that is dominated by radiative recombination of single excitons. At higher fluences, the measured dynamics develop a fast, sub-ns initial component that is due to Auger decay of multiexcitons (*3, 11*). Because of the very short multiexciton lifetimes limited by the Auger process, the PL traces show almost indistinguishable decay for $t > 2$ ns when all of the NCs are occupied with no more than one exciton. By extracting the fast decay component from the PL trace measured using a pump intensity that is just above the onset for the generation of multiexcitons (*3*), we derive the biexciton lifetime (τ_2) ~200 ps (inset of Fig. 2A). This lifetime is consistent with previous studies of CdSe NCs (*3, 11*).

The PL time transients measured for the g-NC sample (Fig. 2B) exhibit very different multiexciton dynamics. As in the reference sample, the low-pump-intensity decay in g-NCs is dominated by single excitons with a lifetime, τ_1, of 42 ns. At higher excitation intensities, the recorded traces again develop a faster multiexcitonic component, but in this case, it persists for much longer than in the reference NCs and has an appreciable amplitude even at t = 30 ns after excitation. Based on the measured dynamics, we derive a biexciton lifetime (τ_2) of 10 ns (inset of Fig. 2B). This value is 50 times longer than in the reference sample and, thus, indicates very significant *suppression* of Auger recombination.

On the basis of existing models of radiative decay in NCs, the radiative lifetime of a biexciton (τ_{2r}) is shorter than that of a single exciton (τ_{1r}) by a factor of 2 (for independent excitons) to 4 (for bulk-like recombination) (*18*). From PL relaxation measured at low pump fluences, τ_{1r} = 42 ns, and hence, the expected value of τ_{2r} ranges from 21 to 10.5 ns. Both of these values are comparable to the newly measured 10-ns biexciton lifetime. This key result implies that the biexciton decay is either purely radiative (if τ_{2r} = 10.5 ns then $\tau_{2A} >> \tau_{2r}$, where τ_{2A} is the biexciton Auger recombination lifetime) or only weakly affected by extremely slow Auger recombination (if τ_{2r} = 21 ns then τ_{2A} = 19 ns).

Very long multiexciton lifetimes are also evident from pump-intensity dependent studies of PL (Figs. 2C and 2D). In the reference NCs, pump-intensity dependences of PL signals measured at different times after excitation are indistinguishable at $t >> \tau_{2A}$. In this case, all of the multiexcitons have decayed via the Auger process and the emission intensity is simply determined by the total number of photo-excited NCs independent of their early time occupancies. This behavior is evident from the data in Fig. 2C, where the pump-intensity dependences recorded at $t \geq 2$ ns converge to a single saturation curve independent of the exact

delay time used in the PL measurements. As expected, the measured long-lived PL signals closely follow the pump-intensity-dependent evolution of the total number of photoexcited NCs calculated assuming Poisson statistics of photon absorption events (red solid line in Fig. 2C): $I_{PL}(t >> \tau_2) \propto (1 - p_0) = (1 - \exp(-\langle N_0 \rangle)$, where p_0 is the fraction of unexcited NCs (*19*).

The situation is clearly different for g–NCs (Fig. 2D). Specifically, in this case, the PL pump-intensity dependence evolves on a much longer time scale and "stabilizes" only at $t > 50$ ns. This slow evolution is a result of the slow decay of multiexcitons. Because of their contribution to emission, the PL pump-intensity dependences measured at $t < 50$ ns significantly deviate from the $1 - p_0$ Poisson term (red solid line in Fig. 2D). Only at very long times ($t > 60$ ns) does the PL intensity exhibit the $(1- p_0)$ dependence, indicating that all of the multiexcitons have finally decayed and only single excitons are present in the system.

There are several factors that can potentially lead to suppression of Auger recombination in g-NCs: changes in the effective extent of electronic wave functions, altered electron-hole overlap and exciton-exciton repulsion, and/or the influence of interfaces. We consider each here. Typically, Auger rates are inversely proportional to NC volume (*3, 11*). Therefore, the large spatial extent of the electronic wave functions in g-NCs is expected to lead to increased biexciton lifetimes. Based on effective volume considerations, the biexciton lifetime in g-NCs should be comparable to that in the reference NCs because these two types of NCs are characterized by similar degrees of spatial confinement of electronic excitations (as indicated by the similarity of their emission wavelengths). Despite these expectations, however, the reference and g-NC samples show a dramatic, 50-fold difference in biexciton lifetimes (200 ps vs. 10 ns, respectively), which implies that effective volume arguments alone cannot explain slowing of multiexciton dynamics in g-NCs.

Second, as was mentioned earlier, g-NCs exhibit partial spatial separation between electrons and holes (holes are confined to the g-NC core while electrons are delocalized over its entire volume). This situation results in a reduced electron-hole overlap integral (θ_{eh}) that could decrease the rate of Auger decay (*13, 20*). In our case, however, the calculated value of θ_{eh} is still on the order of ~0.6 (inset of Fig. 1F), which is not sufficiently small to explain the 50-fold increase in the biexciton lifetime.

Thirdly, we consider exciton-exciton repulsion (*21, 22*). As mentioned previously, this effect is possible in heterostructures that are characterized by either complete (type-II) or partial (quasi-type-II) spatial separation between electron and hole wave functions (*21*). In such nanostructures, repulsive Coulomb interactions provide an additional driving force that together with an energy gradient at a hetero-interface, helps to keep electrons and holes apart, thereby reducing the rate of Auger recombination. Our calculations predict that the partial spatial separation between electrons and holes occurring in g-NCs can indeed produce appreciable exciton-exciton repulsion (see Fig. S2B in SOM). This effect is evident from the measured time-resolved PL spectra that indicate a transient red shift of the PL maximum (inset of Fig. 2D). The fact that multiexciton recombination is accompanied by a decrease in the emission energy implies that the average per-exciton energy in a multiexciton is higher than that of a single exciton. Such an observation is a signature of exciton-exciton repulsion (*13, 22*). While the above measurements clearly show the existence of exciton-exciton repulsion in g-NCs, they also indicate that the repulsion energy is quite small (~10 meV; see Fig. 2SB in SOM) and, hence, cannot significantly affect Auger recombination. For example, even in type-II CdS/ZnSe NCs with a Coulomb repulsion energy on the order of 100 meV (*13, 22*), Auger recombination still occurs on a sub-ns time scale (*13*).

The large nanoparticle size, charge separation and Coulomb repulsion that we have measured in g-NCs may indeed have an important contribution to the suppression of Auger recombination when all these effects are taken in aggregate. However, the effect of NC interfaces on Auger decay rates may also play a particularly important role in g-NCs. According to Efros (*23*), Auger recombination in NCs primarily takes place at interfacial regions and the likelihood of this process is directly dependent on the steepness of the interface potential. The difference in interfacial properties may, for example, explain a dramatic distinction in multiexciton dynamics in colloidal and epitaxial quantum dots. It is well-established that Auger recombination is not efficient in quantum dots fabricated by physical methods such as molecular beam epitaxy (*24*), while it is extremely fast and efficient in colloidal NCs (*3*). Epitaxial dots are typically embedded in a matrix of a wide-gap semiconductor such as ZnSe at temperatures high enough to produce interfacial alloying (*25, 26*). The "smoothness" of the resulting interfacial potential can be responsible for suppression of Auger recombination in these structures. This situation is in contrast to typical colloidal NCs that are characterized by sharp interfaces (semiconductor/solvent or semiconductor/ligands) with very large energy gradients. The interfacial properties of g-NCs are likely similar to those of epitaxial dots. Despite a moderate growth temperature (240 ^{o}C), the long reaction time (it takes ~40 hours to fabricate a sample with a 10 monolayer CdS shell) can lead to significant inter-diffusion of anions between the core and the shell, which could result in the formation of an intermediate alloyed layer with a smoothed potential.

The suppression of Auger recombination can greatly benefit NC lasing applications. If exciton-exciton coupling is neglected, optical gain in NCs necessarily involves stimulated emission from multiexciton states (*4, 13*). In this case, optical gain dynamics are usually

controlled by Auger recombination, which limits the optical-gain lifetime to tens of picoseconds. Auger recombination also imposes severe constraints on the spectral bandwidth of optical amplification. Optical gain due to biexcitons has a spectral width that is typically just a small fraction of the total width of the band-edge spontaneous PL (*4*). The extension of optical gain to higher energies is only possible through stimulated emission by higher-order multiexcitons. Such multiexcitons, however, have lifetimes that are even shorter than those of biexciton states. This is because of the rapid scaling of Auger rate with the number of multiexcitons (*N*). For instance, in CdSe NCs it changes from quadratic to cubic with increasing NC size (*11*). As a result, optical gain due to higher-order multiexcitons is extremely short-lived and typically not usable for optical amplification. Therefore, most reports on optical amplification in NCs only show ASE due to the lowest-energy band-edge transition and very few studies (*27, 28*) have demonstrated ASE due to transitions that also involve the first excited electron state.

Based on the observations of long multiexciton lifetimes in g-NCs, one may expect that these samples could allow for extension of optical amplification bandwidth through the involvement of higher-order multiexcitons. Such spectral extension is indeed observed experimentally. The results of our ASE studies for g-NCs with an 11 monolayer shell in a close-packed film are summarized in Fig. 3. At low excitation fluences, we observe spontaneous band-edge emission at 1.95 eV. At a fluence of 30 $\mu J\ cm^{-2}$, a narrower peak develops on the higher energy side (1.99 eV) of the spontaneous emission band (Fig. 3A), that together with a super-linear dependence on pump fluence (Fig. 3B) indicates the ASE process. The blue shift of this ASE feature with regard to the spontaneous emission band is consistent with a repulsive character of exciton-exciton interactions in the g-NCs as discussed above.

As the pump fluence increases further, we detect two higher-energy ASE peaks (at 2.19 eV and 2.34 eV) that are likely due to optical transitions involving the first and the second excited electron states, respectively. Within a simple particle-in-a-box model (*29*), the second excited state becomes occupied only if the NC contains at least 9 excitons. This value is consistent with the pump fluence that is required to excite the third ASE feature, which corresponds to $\langle N_0 \rangle \sim 11$. These observations imply that multiexcitons of the 9th order (and possibly even higher) are sufficiently long lived in g-NCs to produce the ASE effect.

As a result of the participation of higher-order multiexcitons, the optical gain of g-NCs in a dilute solution measured using transient absorption exhibits an unprecedented bandwidth of ~500 meV (Fig. 3C). This large bandwidth is highly unusual not only for NC samples (open circles in Fig. 3C) but also for other typical gain media such as laser dyes (dye gain bandwidths are typically <300 meV). These results imply that using a single g-NC sample one can tune the lasing color almost over the entire range of visible wavelengths by simply adjusting a laser cavity (Fig. S3). Furthermore, such bandwidth is sufficiently large to support femtosecond laser pulses.

The g-NC samples also show remarkably low ASE thresholds that result from increased absorption cross-sections in addition to suppressed Auger decay. Specifically, in a reference NC sample, the excitation threshold for the band edge biexcitonic ASE is ~300 $\mu J\ cm^{-2}$, while it is only ~26 $\mu J\ cm^{-2}$ in g-NCs (squares in Fig. 3B). Interestingly, excitation thresholds for the second (~100 $\mu J\ cm^{-2}$) and the third (~220 $\mu J\ cm^{-2}$) ASE features, which are due to higher–order multiexcitons, are still lower than that for biexcitonic gain in the reference sample.

In conclusion, we show that g-NCs consisting of a small CdSe core overcoated with a thick CdS shell show very long multiexciton lifetimes (~10 ns for a biexciton state) that indicate a

significant, possibly complete, suppression of Auger recombination in these nanostructures. We discuss possible reasons for this suppression including the large effective volume of these NCs and a peculiar spatial distribution of electronic wave functions, which results in reduced electron-hole overlap and weak exciton-exciton repulsion. We conclude that while the above factors could indeed provide some reduction of Auger recombination rates, there may also be an important contribution from a smooth interfacial potential resulting from the formation of a gradient alloy layer at the core/shell interface. This would be analogous to the situation in epitaxial quantum dots, where Auger recombination is an inefficient process. As a final proof of suppression of Auger recombination, we conduct ASE experiments. The ASE measurements indicate an extraordinarily large bandwidth of optical gain (> 500 meV) that results from contributions of multiexcitons of high order (at least 9^{th} and greater) to stimulated emission (*30*).

Figure captions

Fig. 1. (**A**) A schematic of the g-NC structure where R is the CdSe core radius and H is the CdS shell thickness. (**B**) A transmission electron microscopy image of g-NCs with R = 1.5 nm and H = 7.8 nm. Blue lines in the expanded view on the right illustrate a relative size of a core compared to the total size of a g-NC. (**C**) PL (solid black line) and absorption (dashed red line) spectra for CdSe only-core NCs. (**D**) Upon growing a 5.7-nm thick shell of CdS on the CdSe cores shown in panel C, the PL red shifts by ~200 meV and the absorption becomes dominated by the CdS shell. Inset: the PL excitation spectrum (monitored at 1.95 eV), which shows the structure of band-edge transitions due to a CdSe core. (**E**) Band alignment diagram of bulk CdSe and CdS. (**F**) Spatial probability distribution of the hole (dark grey area) and electron (light grey area) for R = 1.5 nm and H = 5.0 nm. The inset shows a contour plot of the calculated electron-hole overlap integral. White and black lines are boundaries between regions of (R,H)-space that correspond to different localization regimes. These lines are calculated from the condition that the probabilities of finding an electron (white dashed line) or a hole (black dashed line) in the core and the shell are equal to each other. The shaded elliptical area shows an approximate range of parameters of g-NCs studied in this work.

Fig. 2. (**A**) Time-resolved PL intensity of reference CdSe/ZnS core-shell NCs (dilute hexane solution) emitting at 1.92 eV for different excitation fluences (2 to 200 $\mu J/cm^2$); pump photon energy is 3.1-eV. Traces normalized at t = 60 ns completely overlap at t > 2 ns, indicating that relatively early in time all of the multiexcitons have already decayed. Inset: the extracted biexciton dynamics shows the 200 ps decay due to Auger recombination. (**B**) The same for g-NCs (12 monolayer CdS shell); PL is monitored at 2.00 eV. Traces normalized at t = 90 ns

become indistinguishable only for $t > 40$ ns, indicating that in this case multiexcitons are long lived. Inset: The extracted biexciton dynamics shows slow 10 ns decay. (**C**) PL intensity for reference CdSe/ZnS NCs as a function of NC average occupancy, $\langle N_0 \rangle$, measured at different times after excitation (symbols). Because of rapid Auger recombination of multiexcitons, the PL intensity saturates according to $(1 - p_0)$ (shown by the red line) for times longer than the biexciton lifetime. As a result, the dependences measured at $t = 2$ ns and 80 ns are almost identical. (**D**) The same for g-NCs. Here, the PL intensity also exhibits saturation but at much longer times ($t > 60$ ns) owing to the dramatically increased lifetime of multiexcitons. The inset shows a transient red shift of the emission maximum as a function of time for $\langle N_0 \rangle = 0.7$. This red shift is a signature of exciton-exciton repulsion.

Fig. 3. (**A**) Emission spectra of a close-packed film of g-NCs (11 monolayer CdS shell) measured using 3.1 eV, 100 fs pump pulses with different per-pulse fluences (indicated in the figure); the pump-spot diameter is 60 μm. These spectra illustrate the development of three ASE peaks at 1.99 eV, 2.19 eV and 2.34 eV that span the range of colours from red to green. (**B**) Emission intensity versus pump fluence at the positions of three ASE peaks observed for g-NCs (solid symbols) in comparison to the pump-fluence-dependent PL intensity for reference CdSe/ZnS NCs (hollow diamonds). (**C**) A normalized transient absorption spectrum of g-NCs (dilute hexane solution) shortly after excitation ($t = 2$ ps) with 3.1 eV, 1.2 mJ cm^{-2} pulses (red solid circles); this spectrum is calculated as a ratio of the measured pump-induced absorption bleaching ($\Delta\alpha < 0$) and ground-state absorption (α_0). In this representation, optical gain corresponds to the situation where $-\Delta\alpha/\alpha_0 > 1$. Black open circles show the same type of spectrum for core-only CdSe NCs recorded using similar excitation conditions.

Supporting Online Material

www.sciencemag.org

SOM text

Fig. S1 to S3

Table S1

References

Figures

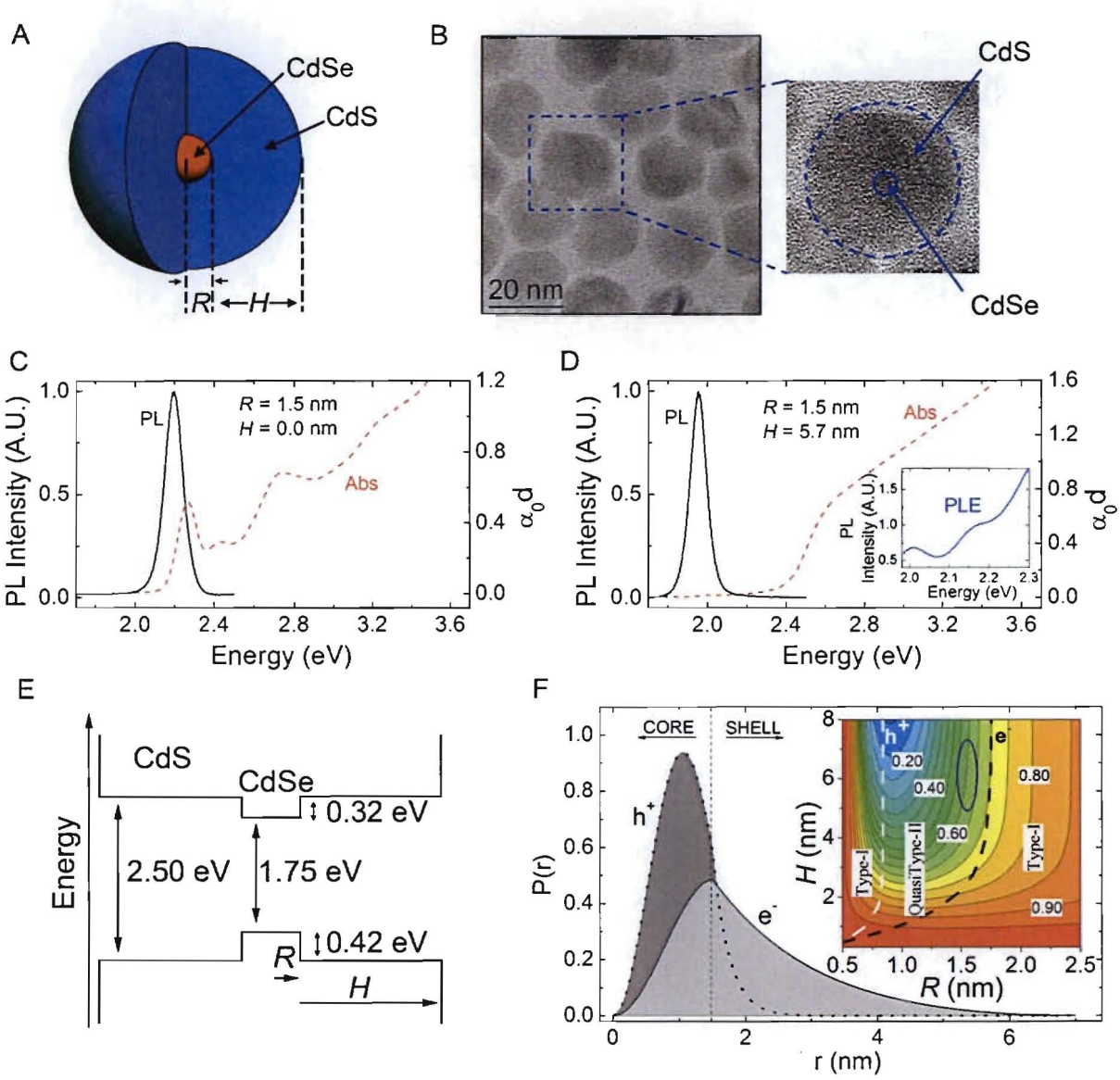
A
CdSe
CdS
R
H
B
CdS
20 nm
CdSe
C
PL Intensity (A.U.)
PL
R = 1.5 nm
H = 0.0 nm
Abs
$\alpha_0 d$
Energy (eV)
D
PL Intensity (A.U.)
PL
R = 1.5 nm
H = 5.7 nm
Abs
PLE
PL Intensity (A.U.)
Energy (eV)
$\alpha_0 d$
Energy (eV)
E
Energy
CdS
CdSe
0.32 eV
2.50 eV
1.75 eV
0.42 eV
R
H
F
CORE
SHELL
h+
e-
P(r)
r (nm)
H (nm)
R (nm)
0.20
0.40
0.60
0.80
0.90
Type-I
QuasiType-II
Type-I

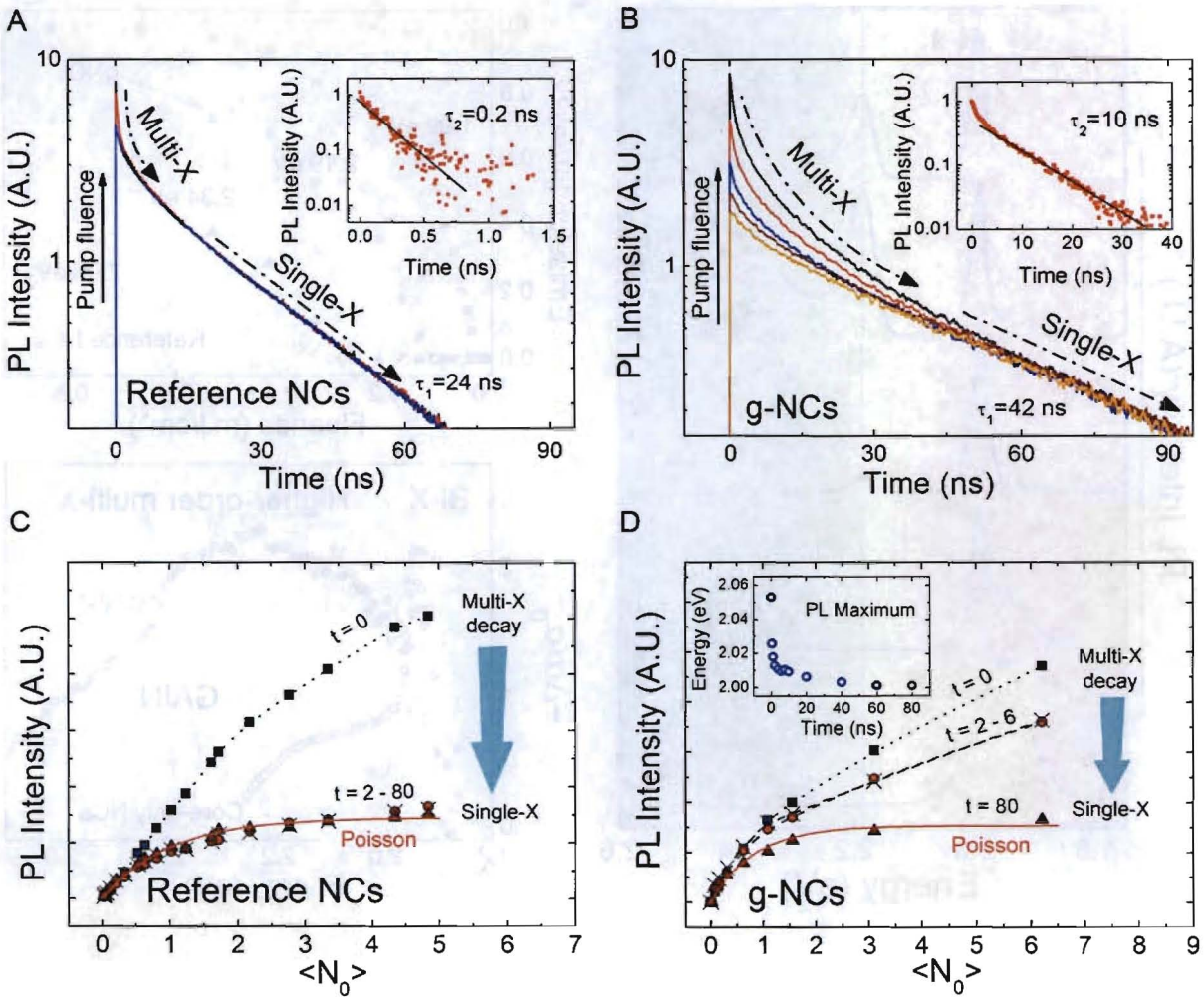
A
PL Intensity (A.U.)
Pump fluence
Multi-X
Single-X
Reference NCs
τ1=24 ns
Time (ns)
PL Intensity (A.U.)
τ2=0.2 ns
Time (ns)
B
PL Intensity (A.U.)
Pump fluence
Multi-X
Single-X
g-NCs
τ1=42 ns
Time (ns)
PL Intensity (A.U.)
τ2=10 ns
Time (ns)
C
PL Intensity (A.U.)
Multi-X decay
t = 0
t = 2 - 80
Single-X
Poisson
Reference NCs
<N0>
D
PL Intensity (A.U.)
Energy (eV)
PL Maximum
Time (ns)
Multi-X decay
t = 0
t = 2 - 6
t = 80
Single-X
Poisson
g-NCs
<N0>

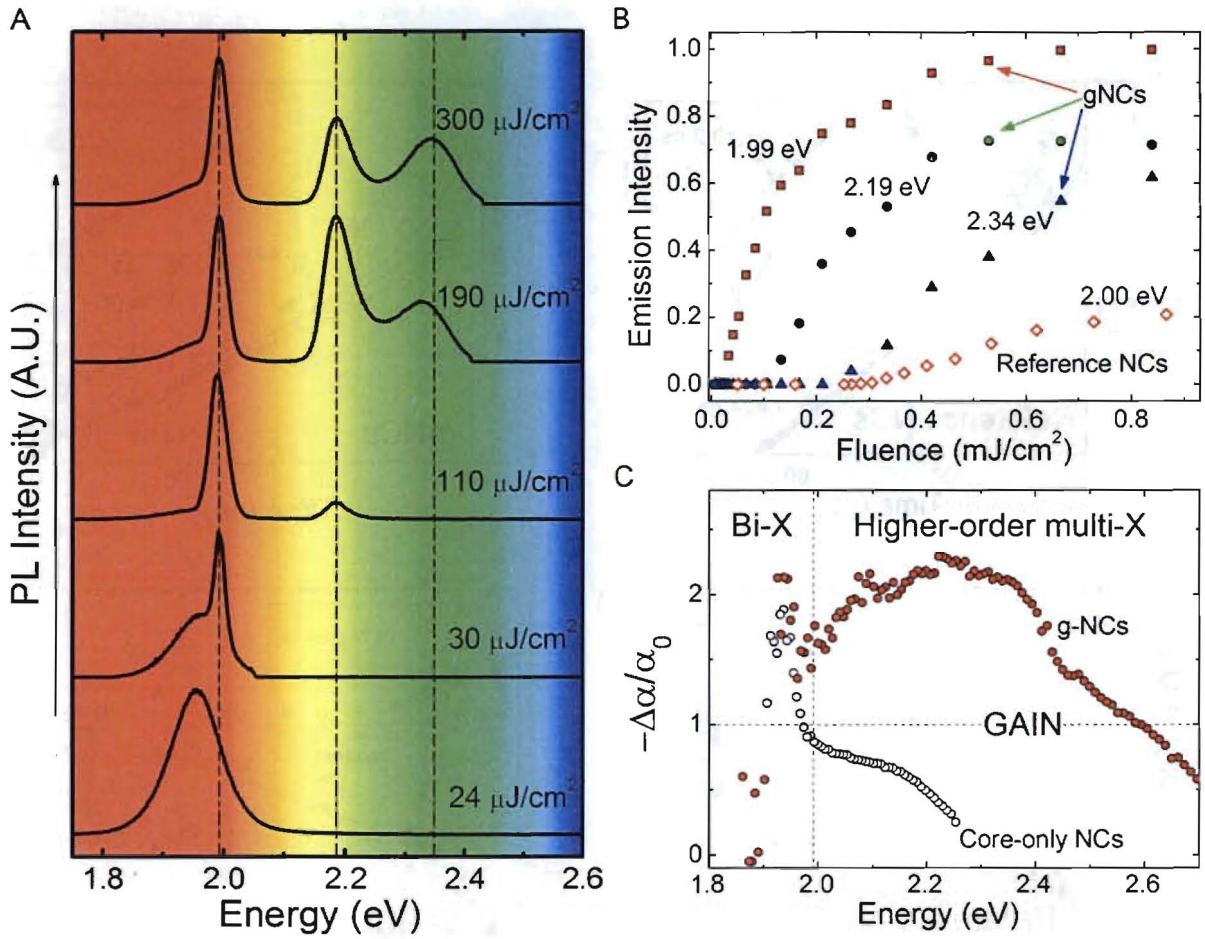
A
PL Intensity (A.U.)
300 μJ/cm²
190 μJ/cm²
110 μJ/cm²
30 μJ/cm²
24 μJ/cm²
1.8
2.0
2.2
2.4
2.6
Energy (eV)
B
Emission Intensity
gNCs
1.99 eV
2.19 eV
2.34 eV
2.00 eV
Reference NCs
Fluence (mJ/cm²)
C
Bi-X
Higher-order multi-X
g-NCs
GAIN
Core-only NCs
$-\Delta\alpha/\alpha_0$
Energy (eV)

References and Notes

1. A. P. Alivisatos, *Science* **271**, 933 (1996).

2. V. I. Klimov, *Semiconductor and metal nanocrystals* (Marcel Dekker, New York, 2004)

3. V. I. Klimov, A. A. Mikhailovsky, D. W. McBranch, C. A. Leatherdale, M. G. Bawendi, *Science* **287**, 1011 (2000).

4. V. I. Klimov *et al.*, *Science* **290**, 314 (2000).

5. A. J. Nozik, *Physica E* **14**, 115 (2002).

6. P. O. Anikeeva, C. F. Madigan, J. E. Halpert, M. G. Bawendi, V. Bulovic, *Phys. Rev. B* **78**, 8 (2008).

7. M. Nirmal *et al.*, *Nature* **383**, 802 (1996).

8. A. L. Efros, M. Rosen, *Phys. Rev. Lett.* **78**, 1110 (1997).

9. D. I. Chepic *et al.*, *J. Lumines.* **47**, 113 (1990).

10. L. W. Wang, M. Califano, A. Zunger, A. Franceschetti, *Phys. Rev. Lett.* **91**, 4 (2003).

11. V. I. Klimov, J. A. McGuire, R. D. Schaller, V. I. Rupasov, *Phys. Rev. B* **77**, 12 (2008).

12. H. Htoon, J. A. Hollingsworth, R. Dickerson, V. I. Klimov, *Phys. Rev. Lett.* **91**, 4 (2003).

13. J. Nanda *et al.*, *J. Phys. Chem. C* **111**, 15382 (2007).

14. J. Nanda *et al.*, *J. Appl. Phys.* **99**, 7 (2006).

15. Y. Chen *et al.*, *J. Am. Chem. Soc.* **130**, 5026 (2008).

16. B. Mahler *et al.*, *Nat. Mater.* **7**, 659 (2008).

17. M. A. Hines, P. Guyot-Sionnest, *J. Phys. Chem.* **100**, 468 (1996).

18. J. A. McGuire, J. Joo, J. M. Pietryga, R. D. Schaller, V. I. Klimov, *Accounts Chem. Res.* **41**, 1810 (2008).

19. V. I. Klimov, *J. Phys. Chem. B* **104**, 6112 (2000).

20. D. Oron, M. Kazes, U. Banin, *Phys. Rev. B* **75**, 7 (2007).

21. A. Piryatinski, S. A. Ivanov, S. Tretiak, V. I. Klimov, *Nano Lett.* **7**, 108 (2007).

22. V. I. Klimov *et al.*, *Nature* **447**, 441 (2007).

23. A. L. Efros, in *Semiconductor nanocrystals,* A. L. Efros, D. J. Lockwood, L. Tybeskov, Eds. (Kluwer academic/Plenum Publishers, New York, 2003), chap. 2.

24. E. Dekel *et al.*, *Phys. Rev. Lett.* **80**, 4991 (1998).

25. I. Kegel *et al.*, *Phys. Rev. Lett.* **85**, 1694 (2000).

26. N. Liu, J. Tersoff, O. Baklenov, A. L. Holmes, C. K. Shih, *Phys. Rev. Lett.* **84**, 334 (2000).

27. H. Htoon, J. A. Hollingworth, A. V. Malko, R. Dickerson, V. I. Klimov, *Appl. Phys. Lett.* **82**, 4776 (2003).

28. Y. Chan, J. M. Caruge, P. T. Snee, M. G. Bawendi, *Appl. Phys. Lett.* **85**, 2460 (2004).

29. A. L. Efros, A. L. Efros, *Sov. Phys. Semicond.* **16**, 772 (1982).

30. Supported by the Chemical Sciences, Biosciences and Geosciences Division of the Office of Basic Energy Sciences, U.S. Department of Energy (DOE) and Los Alamos LDRD funds. V.I.K. and J.A.H acknowledge partial support from the Center for Integrated Nanotechnologies jointly operated for DOE by Los Alamos and Sandia National Laboratories. J.A.H. also acknowledges partial support from NIH NIGMS grant 1R01GM084702-01. F.G.-S. and J. V. are Los Alamos National Laboratory Director's Fellows.